Rare Metal Materials and Engineering
Volume 51, Issue 12, December 2022
Available online at www.rmme.ac.cn

Science Press

Cite this article as: Li Lei, Guo Dizi, Ying Yang, et al. Research Progress on Crystal Structures and Structural Transformation of Titanium[J]. Rare Metal Materials and Engineering, 2022, 51(12): 4398-4409.

REVIEW

Research Progress on Crystal Structures and Structural Transformation of Titanium

Li Lei[1], Guo Dizi[1], Ying Yang[1], Hong Quan[1], Vincent JI[2]

[1] Northwest Institute for Nonferrous Metal Research, Xi'an 710016, China; [2] Paris-Saclay University, Orsay 91405, France

Abstract: High strength, low density, and excellent corrosion resistance are the main properties making titanium attractive in a variety of applications. The crystal structures and structural transformations of titanium allotropes, which are of tremendous scientific and technological interest, have attracted a great deal of attention for many years. In addition to hexagonal close packed α-Ti, high temperature phase β-Ti with body-centred cubic structure and ω-Ti with the hexagonal structure, researchers have tried to find other metastable structures which can be maintained under extreme conditions through various methods. During the past decades, the ultrahigh pressure structures γ-Ti and δ-Ti are observed, and the room temperature ω-Ti and fcc-Ti can be obtained by high pressure torsion, laser shock, ultra-thin films, etc. The research progress of crystal structures and structural transformations of titanium were introduced. The structural stability and mechanism of structural transformations on titanium were elaborated.

Key words: crystal structure; structural transformation; high pressure; fcc-Ti

Theoretical and experimental studies on crystal structures of elements in the periodic table have been one of the important subjects, which have attracted a great deal of attention for many years. It is generally accepted that crystal structures of transition metals are controlled by the valence d electrons per atom[1,2]. As shown in Table 1[1,3], the structures of all d transition metals (excluding the magnetic d transition metals) tend to have the canonical hcp→bcc→hcp→fcc sequence as their atomic number increases. Because compression can lead to an increase in d-electron population by transfer of electrons from the sp band, similar structure sequences are expected to occur in individual transition metals with increasing pressure. As one of the group IV transition metals, titanium has a narrow d band and a broad sp band. Under pressure, the electrons transferring from the sp band to the d band is considered to be the driving force behind the structural transformations. The pressure-induced structural transformation of titanium was first observed by Jamieson in 1963[4], and investigated extensively both in theories[3,5-13] and experiments[14-24].

According to the above principle, the crystal structure of group IV transition metals (Ti, Zr, Hf) should transform to the structure of neighbouring group V transition metals (bcc structure) under high pressure. The first-principles calculations predicted that the pressure-induced structural transformations of group IV transition metals should undergo a $\alpha \rightarrow \omega \rightarrow \beta$ transformation sequence with increasing pressure[4]. The room temperature high-pressure experimental studies showed similar $\alpha \rightarrow \omega$ transformation in Ti, Zr and Hf at 2~38 GPa[2,4,14-22]. Zr and Hf transform to bcc structure at 30 and 71 GPa[2,17]. Although the calculations predicted that the onset pressure of $\omega \rightarrow \beta$ transformation of Ti will be 57.5[4] or 80 GPa[8], actually the β-Ti has not been detected even under 220 GPa[20]. Similarly, the pure bcc-Zr was formed by high pressure torsion (HPT) experiment[25,26]. But, so far, only room-temperature ω-Ti can be observed in HPT processing. The β-Ti has still not been detected even under extreme conditions[27-33]. The room-temperature β-Ti is always of great interest in the research on structural transformations of Ti.

Ultrathin film (especially epitaxial film) is another actively pursued area of research on crystal structures and structural transformations[34-37]. The epitaxial growth of metal film can always match the lattice of substrates and form metastable phase which is normally different from the structure in bulk

Received date: July 27, 2022
Foundation item: National Nature Science Foundation of China (51201138); International Science & Technology Cooperation Program of Shaanxi Province (2022KW-41, 2020KW-040)
Corresponding author: Li Lei, Ph. D., Senior Engineer, Northwest Institute for Nonferrous Metal Research, Xi'an 710016, P. R. China, Tel: 0086-29-86250729, E-mail: lilei@c-nin.com

Table 1 Crystal structures of the d transition metals[1,3]

Group	III B	IV B	V B	VI B	VII B	VIII			I B	II B
3d, 4s	Sc	Ti	V	Cr	Mn	Fe	Co	Ni	Cu	Zn
	hcp	hcp	bcc	bcc	(bcc)	bcc	hcp	fcc	fcc	hcp
4d, 5s	Y	Zr	Nb	Mo	Tc	Ru	Rh	Pd	Ag	Cd
	hcp	hcp	bcc	bcc	hcp	hcp	fcc	fcc	fcc	hcp
5d, 6s	[La]	Hf	Ta	W	Re	Os	Ir	Pt	Au	Hg
	hcp	hcp	bcc	bcc	hcp	hcp	fcc	fcc	fcc	(fcc)
			hcp →	bcc →	hcp →	fcc →	hcp			

materials. A face centred cubic structure (fcc-Ti), which is not arisen in P-T diagram, was first observed in ultrathin films on NaCl substrate by wawner[38]. From then on, the fcc-Ti films on different kinds of substrates have been investigated[39-56]. While the first-principles study revealed that the total energy of the fcc-Ti is significantly higher than that of the α-Ti and ω-Ti even with a volume reduction of 15%[57].

Titanium is recognized for its highest strength-to-weight ratio among all metals. Elevated temperature property is also an outstanding merit compared with other metals. Chemically, the excellent resistance to corrosion is the most noted property of titanium. Because of these unique properties, titanium and its alloy are widely used in aerospace, military, petrochemicals, automotive and nuclear fields. However, titanium parts always work in abominable conditions, such as high pressure or tension, high pressure shock, high temperature impact. These external environmental factors may induce structural transformations which can change the physical properties of titanium parts. In the aerospace industry, the pressure-induced $\alpha \rightarrow \omega$ structural transformation in pure titanium and titanium alloys have significant implications, because the ω-Ti affects the toughness and ductility of titanium parts[3]. Other crystal structures of titanium, such as β-Ti, which has been calculated to have a lower elastic modulus than α-Ti [58], may be applied to bone implants materials. The β-Ti has been predicted to have much higher superconducting transition temperatures (T_c) (0.4 and 0.6 K for α-Ti and α-Zr, respectively; T_c of β-Zr is measured to be 11 K[59]), which has been attributed to the increasing occupancy of the d band[60]. Therefore, the research on crystal structures and structural transformations of titanium has tremendous scientific and technological interest.

The present study deals with the developments of the preparation of metastable structures and structural transformations of titanium. The crystal parameters and XRD patterns of the structures of titanium are listed. Various experimental methods for preparing titanium metastable phases are introduced, such as adjusting temperature, static pressure, high pressure torsion, shock load, thin film preparation. The preparation methods of fcc-Ti which is not present in P-T diagram are introduced in detail. The structure stability and mechanism of structural transformations of titanium are elaborated.

1 Crystal Structures of Titanium

1.1 Structure parameters of titanium

In addition to α, β, ω structures, two structures were observed when the pressure increased to 118 GPa[19] for γ phase and 140 GPa for δ phase[20]. Furthermore, fcc-Ti was reported in thin epitaxial films[38,57]. So far, the crystal structures of titanium allotropes as known contain α, β, ω, γ, δ and fcc. The space group and lattice constants data of these structures under specific conditions are shown in Table 2.

It should be noted that only the crystal structures in pure titanium without any alloying element were investigated in this work. The phase structures which are observed in titanium alloy[62-64], such as α', α'', α_2, β', β_2, γ-TiAl, O, $B8_2$, are not discussed here.

The unit cell of α-Ti contains a total of two atoms, occupying (1/3, 2/3, 1/4), (2/3, 1/3, 3/4) position, and c/a is about 1.58. The β-Ti unit cell contains two atoms, which are located at (0, 0, 0) and (1/2, 1/2, 1/2).

There are two slightly different modifications of ω-Ti. One is the ideal ω structure with hexagonal symmetry, and the

Table 2 Lattice constants of Ti allotropes

Phase structure	Crystal structure	Space group	Lattice parameter/nm	Note
α	Close-packed hexagonal	194 P63/MMC	a = 0.295 05, c=0.468 26	RT, 101.325 kPa[37]
β	Body-centered cubic	229 IM-3M	a=b=c=0.330 65	900 °C, 101.325 kPa[37]
ω	Hexagonal-ω	191 P6/MMM	a=0.460, c=0.282	RT, 101.325 kPa[61]
	Trigonal-ω	164 P-3M1	a=0.460, c=0.282	
γ	Orthorhombic	63 CMCM	a=0.2388, b=0.4484, c=0.3915	RT, 118 GPa[19]
δ	Orthorhombic	63 CMCM	a=0.3861, b=0.2630, c=0.3632	RT, 140 GPa[20]
fcc	Face-centered cubic	225 FM-3M	a=b=c=0.416	RT, 101.325 kPa[57]

other is trigonal ω structure. The hexagonal ω structure has three Ti atoms per unit cell, one in A-plane and two in B-plane. The atomic position is (0, 0, 0), (1/3, 2/3, 1/2), (2/3, 1/3, 1/2), and c/a is about 0.612. The trigonal ω structure is similar to hexagonal structure, except that the atoms in B-plane are displaced slightly out of the (0001) plane, alternatively up and down in the direction of the c-axis. The atomic position is (0, 0, 0), (1/3, 2/3, 1/2+Z), (2/3, 1/3, 1/2-Z), where $0<Z<0.167$. When Z=0, the structure becomes hexagonal ω, and the structure goes to bcc at Z=0.167. The packing ratio of the ω structure is only 0.57, which is substantially lower than that of β-Ti (0.68) and α-Ti (0.74).

The γ and δ phases are ultrahigh pressure metastable phases with orthorhombic structure, and the space group are CMCM. Each of the original cell has 4 atoms, and the atomic positions are (0, y, 1/4), (0, -y, 3/4), (0, y, 1/4), (0, y, 1/4); for γ phase y= 0.11, and for δ phase y=0.30[20].

1.2 Measurement of structural transformation

XRD measurement is a convenient way to determine the crystal structures. Fig. 1 shows the XRD patterns of α, β, ω (hexagonal- ω) and fcc structures which are calculated by commercial software using lattice parameter given in Table 2. The crystal structures can also be determined by selected area electron diffraction (SAED) and high-resolution transmission electron microscopy (HRTEM). The SAED and HRTEM images in Fig. 6, Fig. 9 and Fig. 11 can further confirm the metastable structures.

In addition, the differences of physical properties of different structures can also be measured as sensitive probes for detecting structural transformations. For example, early researches detected transformations in titanium by high pressure resistance measurement, because the resistance of the ω-Ti is obviously larger than that of α-Ti. As shown in Fig.2a, the thermal stability of metastable ω-Ti can also be investigated by measuring the electrical resistivity[14,31]. The microhardness of room-temperature ω-Ti is almost two times that of α-Ti, and is reduced to that of α-Ti at high temperature when $\omega \rightarrow \alpha$ back transformation takes place[65] (Fig. 2b). The aggregate sound velocities of Ti are sensitive to change in structure. With increasing pressure, the compressional and shear sound velocities of α-Ti and ω-Ti were calculated to have obvious differences[66]. The acoustic velocity measurement can detect the solid-solid structural transformation of Ti during high pressure.

2 Structural Transformations of Titanium

2.1 Temperature-induced structural transformation

Titanium can crystallize in various crystal structures, which depends on the environment conditions. However, each structure is only stable within particular temperature ranges. It is well known that the α-Ti transforms to β-Ti at temperature higher than 882 °C. This temperature-induced $\alpha \rightarrow \beta$ structural transformation is of central importance to the hot working, since the ease of plastic deformation increases from the hcp lattice to the bcc lattice, which is due to the number difference of slip systems between different structures.

The room-temperature ω-Ti is metastable, and the thermal stability studies of ω -Ti display $\omega \rightarrow \alpha$ structural transformation at elevated temperatures. Fig. 2a shows the variation of electrical resistivity with heating temperature. The electrical resistivity of HPT-processed ω-Ti sample drastically decreases at 400~420 K, because of a reverse $\omega \rightarrow \alpha$ transformation[31].

In addition, the crystal structures of metals are determined by the total electronic energy at low temperature. From the first-principles total-energy calculations in a generalized gradient approximation, the enthalpy of the structures of Ti relative to the enthalpy of β phase under pressure is shown in Fig. 3. The results indicate that the ω-Ti is the most stable structure at 0 K and zero pressure.

2.2 Pressure-induced structural transformation

2.2.1 α–ω transformation under high pressure

The first high pressure study of titanium up to 8~9 GPa was done by Jayaraman et al[14]. A structural transformation was detected by high pressure resistivity measurements, which was thought to be $\alpha \rightarrow \beta$ transitions. However, in the following studies, Jamieson[3] identified the new structure as a simple hexagonal structure (ω-Ti) by high pressure X-ray diffraction technique. Later, Sargent et al[15] treated titanium sample under the pressure as low as 2.8 GPa, and found the ω-Ti particles by electron microscopy studies. The experimental data of $\alpha \rightarrow \omega$ structural transformation under static high pressure obtained by researchers are summarized in Table 3.

The structural transformation pressure of Ti shows a wide

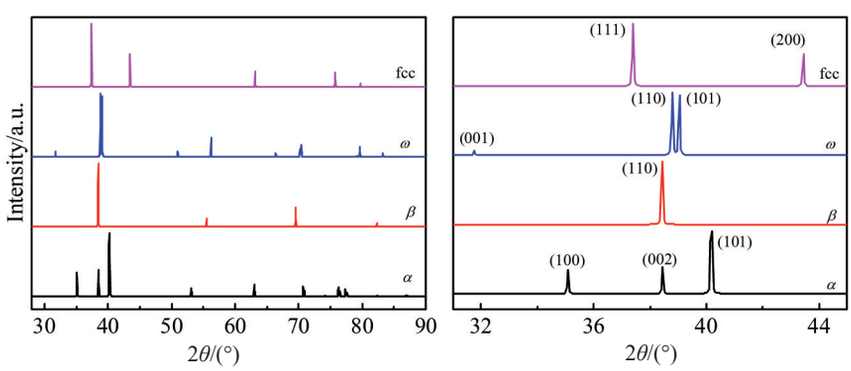

Fig.1 XRD patterns of Ti allotropes

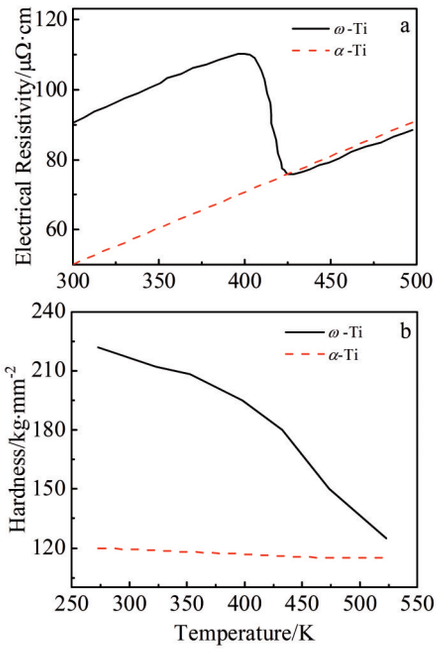

Fig.2 Variation of electrical resistivity (a) and hardness[31] (b) with temperature[65]

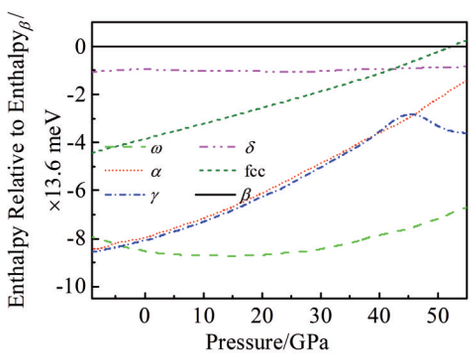

Fig.3 Enthalpy of the allotropes of Ti relative to the enthalpy of β phase under pressure[7]

range of pressure from 2.8 GPa to 14.9 GPa. The big difference of onset transformation pressure of Ti can be attributed to the effects of impurities on the reaction kinetics of $\alpha \rightarrow \omega$ transformation. Vohra et al[68] reported that onset pressure of ω-Ti varies from 2.9 GPa to 6 GPa with increase in oxygen content and other impurity levels in the samples. The ab initio calculations were performed to calculate the effect of impurities on relative energies and energy barriers between α-Ti and ω-Ti. As shown in Table 4, the results reveal interstitial elements (O, N, C), substitution Al, and V interstitials and vacancies, which change the relative energy and the energy barrier and suppress the $\alpha \rightarrow \omega$ transformation[69]. Cerreta et al[70] reported the influence of interstitial O on the propensity of ω-Ti formation in high purity Ti and A-70 alloy (3700 μL/L oxygen) during shock loading. The ω-Ti had not been detected in the A-70 material for shock stresses up to 35 GPa, while the $\alpha \rightarrow \omega$ transformation was found to occur at 10.4 GPa in the high purity Ti.

The model for the formation of ω-Ti from α-Ti was first proposed by Silcock[71]. The $(10\bar{1}0)_\omega$ plane has a similar atomic arrangement to the $(10\bar{1}0)_\alpha$ plane and needs only an expansion of 4% in the $[0001]_\omega$ direction and 2% in the $[1\bar{2}10]$ direction. Vohra et al[72,73] showed the schematic diagram of $\alpha \rightarrow \omega$ transformation in Fig. 4. For the generation of $(11\bar{2}0)_\omega$ plane from the $(0001)_\alpha$ plane, displacement of alternate hexagons on the $(0001)_\alpha$ plane by 0.148 nm is necessary. Further a shortening of ~4.7% along $[11\bar{2}0]_\omega$ and an expansion of ~4.5% along the $[1\bar{1}00]_\alpha$ axis lead to the ω unit cell.

2.2.2 α–ω transformation under superhigh pressure

The results of high-pressure experimental investigations of Zr and Hf are consistent with the expected $\alpha \rightarrow \omega \rightarrow \beta$ structural transformation sequence, which is in qualitative agreement with the first-principles predictions[5]. As to Ti, the theoretical calculations by Ahuja et al[5] predicted $\omega \rightarrow \beta$ transition around 57.5 GPa and a calculated volume compression of V/V_0=0.66. However, the experiment of Xia et al[2] only reported the $\alpha \rightarrow \omega$ transformation up to 87 GPa (volume compression V/V_0= 0.65). Later, Joshi et al[21] raised the transition pressure to 102 GPa based on full-potential linearized augmented plane wave calculations. Then, researchers conducted superhigh pressure experiment to find the expected $\omega \rightarrow \beta$ transformation.

Vohra and Spencer[19] carried out energy dispersive X-ray diffraction studies in megabar pressure experiments, and reported an unexpected structural transformation of Ti from ω to an orthorhombic phase (γ-Ti) at a pressure of 116±4 GPa. Subsequently Akahama et al[20] reported another structural transformation at room temperature from ω to an orthorhombic δ-Ti at 140 GPa via an intermediate γ phase, but the β

Table 3 Summary of $\alpha \rightarrow \omega$ phase transition data of Ti under static high pressure

Transition pressure, $P_{\alpha \rightarrow \omega}$/GPa	ω phase detection technique	Pressure release phase	Ref.
-	X-ray diffraction	ω	[3]
2.8	Electron microscopy	$\alpha+\omega$	[15]
8	Resistivity measurements	-	[8]
8~9	Energy dispersive X-ray diffraction	ω	[2]
4.9~14.9	X-ray diffraction	ω, $\alpha+\omega$	[67]
7.4	Synchrotron X-ray diffraction	ω	[20]
4.9~12.4	Angle dispersive X-ray diffraction	$\alpha+\omega$	[22]
10	X-ray diffraction, resistivity measurements	ω	[23]

Table 4 Change of the relative energy between α and ω ($\Delta E_{\omega\to\alpha}$) and energy barrier ($\Delta E_b$) by impurities in the A-70 and Ti6Al4V alloy[69]

Alloy	Composition/at%	$\Delta E_{\omega\to\alpha}$/meV	ΔE_b/meV
A-70 (commercial Ti alloys)	O 1.10	+12	+10
	N 0.08	+1	+1
	C 0.07	+1	+1
Ti6Al4V	Al 10.70	+29	+31
	V 3.80	-3	-3
	O 0.50	+6	+5

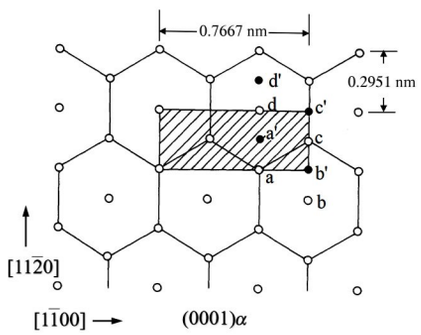

Fig.4 Schematic diagram of $\alpha\to\omega$ transformation (atoms marked as a~d shift to a'~d' to generate ω cell (shaded))[72]

-Ti was not detected until 220 GPa. The pressure dependence of atomic volume for ω, γ and δ structures of Ti is shown in Fig.5[20]. The γ-Ti and δ-Ti are considered as distorted hcp and bcc structures, respectively, which have higher packing ratio than ω-Ti. Therefore, the crystal structures with high packing ratio are expected to appear under superhigh pressure.

Recently, Velisavljevic et al[23] conducted high pressure experiment for nanocrystalline titanium samples, since the decrease in grain size can affect structural stability, kinetics and nucleation/growth of new structures during compression. The results showed similar sequence of $\alpha\to\omega\to\gamma\to\delta$ structural transformation under superhigh pressure up to 161 GPa. So far, to the best of our knowledge, the expected high-pressure β-Ti is still absent.

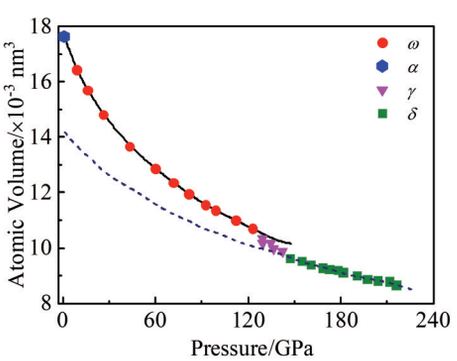

Fig. 5 Pressure dependence of atomic volume for ω, γ and δ structures of Ti at 300 K[20]

2.3 Shear-induced structural transformation

High-pressure torsion is a severe plastic deformation (SPD) method. The number (N) of turns applied to the disc sample and the magnitude of the imposed pressure (P) are key parameters of HPT. The simultaneous application of high pressure and shear stress facilitats the formation of high-pressure phase and stabilization after unloading. Pure β-Zr is fabricated by HPT at room temperature with N=5 and P=3 GPa, while the β-Zr is found at P>30 GPa in high pressure research without shear stress. Moreover, the pure β-Zr is stable at room temperature and atmospheric pressure[25]. Therefore, HPT technique appears to be an ideal process for the research of structural transformation of Ti.

During the past decades, the influence of shear deformation on the structural transformation of Ti was widely investigated. Todaka et al[28] reported the effects of pressure, shear stress and impurity on the $\alpha\to\omega$ structural transformation of HTP processed Ti sample. The XRD peaks of ω-Ti, which is not detected in Ti-0.05%O sample at P=5 GPa without shear stress, appear under torsion strain (N=1/8) at the same pressure. As shown in Fig.6, the increase in the peak intensity of ω-Ti indicates that the $\alpha\to\omega$ structural transformation is stimulated by shear deformation. Comparing Ti-0.05%O and Ti-0.12%O, it is clear that the presence of oxygen suppresses the $\alpha\to\omega$ structural transformation, because oxygen element increases both the ω-Ti energy relative to α-Ti and the energy barrier for the structural transformation.

In addition, HPT process can refine the grain size during

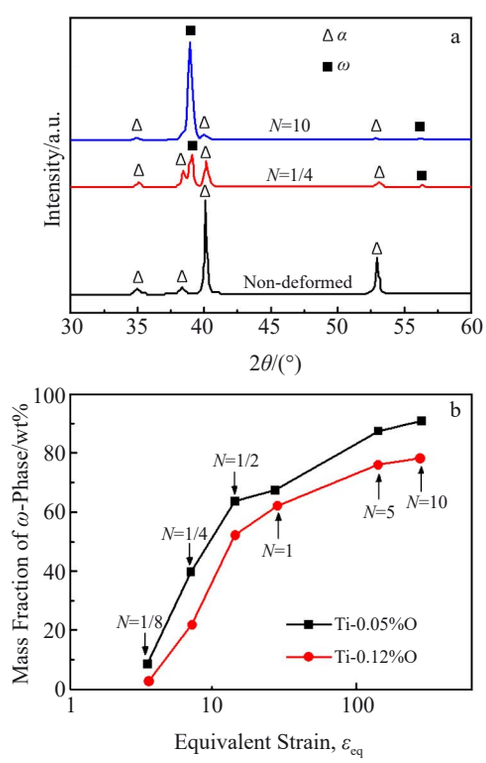

Fig.6 XRD patterns of samples with varying turns of HPT (a) and variation of mass fractions of ω-phase after HPT process with equivalent srtain (b) [43]

deformation, and may introduce grain size-induced structural transformation. Edalati et al[31] reported their study on HPT of Ti at cryogenic and room temperature. Almost a complete $\alpha \rightarrow \omega$ structural transformation occurs under a pressure of 6 GPa at room temperature until the grain size reaches the submicrometer level. The $\alpha \rightarrow \omega$ structural transformation decreases with processing temperature from RT to cryogenic temperature. Moreover, the ω-Ti fraction in HPT sample is found to be related to grain size and the processing temperatures. The grain size effect on $\alpha \rightarrow \omega$ structural transformation is attributed to the significant increase of grain boundaries which may change the relative Gibbs energy of different structures.

2.4 Shock-induced structural transformation

Titanium will undergo $\alpha \rightarrow \omega$ phase transformation under shock load. It is reported that the $\alpha \rightarrow \omega$ phase transformation impact pressure is 5.1~15 GPa[73-77]. The fluctuation of phase transformation impact pressure is related to the experimental methods, which cause differences in the action time, loading mode and other factors of high-pressure impact. Saxena et al[74] conducted impact test with portable electric gun equipment. The phase transformation impact pressure of pure titanium samples with purity of 99.99% is 11.4±1.6 GPa. This is quite different from the 5.1 GPa obtained by Razorenov et al[75] in the impact experiment with Al impactor. The experimental results of Borisenok et al[76] showed that when the impact pressure is 11.5~15 GPa, the ω phase content in matrix increases with the impact pressure. Cerreta et al[70] reported the influence of interstitial O on the propensity of ω-Ti formation in high purity Ti and A-70 alloy (3700 μL/L oxygen) during shock loading. The ω-Ti is not detected in the A-70 material under shock stresses up to 35 GPa, while in the high purity Ti, the $\alpha \rightarrow \omega$ transformation is found to occur at 10.4 GPa. Recently, Zong et al[77] used molecular dynamics simulations to investigate the twin boundary activated $\alpha \rightarrow \omega$ phase transformation in titanium under shock compression. The results showed that the elastic shock wave can readily trigger the $\alpha \rightarrow \omega$ transformation at coherent twin boundaries (CTB), and the phase transformation at CTB leads to considerable wave attenuation.

Our recent research on the effect of laser shock peening (LSP) of the $\alpha \rightarrow \omega$ structural transformation in high-purity titanium revealed that the CTB of nano mechanical twins (MTs) may activate $\alpha \rightarrow \omega$ phase transformation under laser shock impacts[78]. Fig. 7 shows the TEM and HRTEM micrographs and SAED pattern after the first laser shock impact. A large number of high-density dislocations and nano MTs form in the grains. The orientation relationship is $\{0001\}_{\omega}//\{11\bar{2}0\}_{\alpha}$, which is consistent with the Silcock pathway. The $\alpha \rightarrow \omega$ phase transformation in high-purity titanium samples is related to the experimental parameters and the purity of samples. The fraction of transformed ω phase increases with pulse laser energy, pulse width and the number of impacts.

2.5 Crystal structures and transformations in Ti films

Thin film is another actively pursued research on crystal structures and transformations. The growth of metal thin film always forms the metastable structure which is normally different from the structure in bulk materials. This metastable structure can maintain a few monolayers before transforming to equilibrium structure. For ultrathin film, the crystal

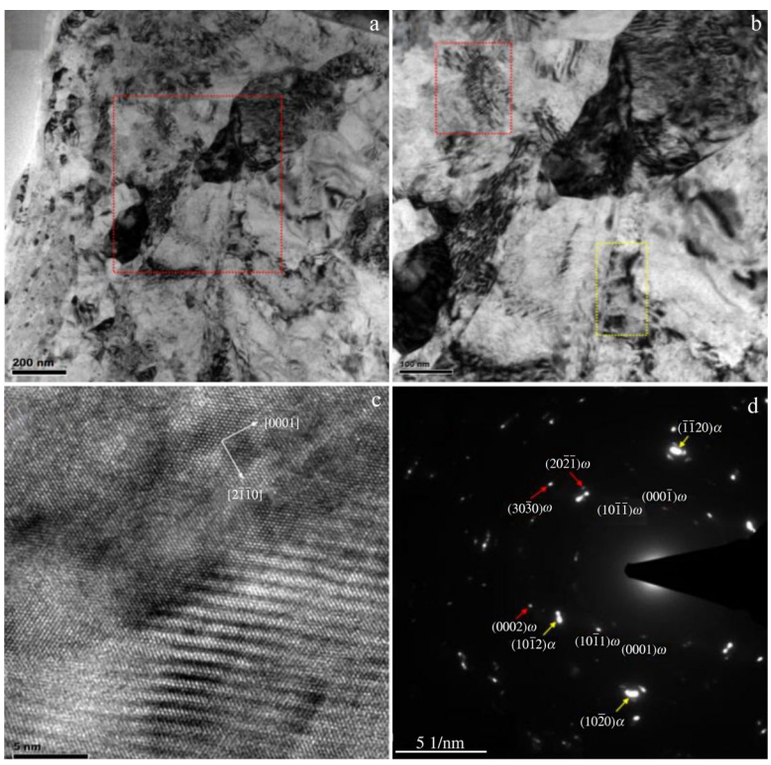

Fig.7 Cross-sectional TEM (a, b) and HRTEM (c) micrographs and SAED pattern (d) of high-purity titanium after laser shock peening

structures of Ti films depend on the growth conditions, such as preparation methods, kinds of substrates, temperature, speed of deposition.

An evaporated Ti film with trigonal-ω structure instead of the normal hcp structure has been reported by Cheng and Meng[37]. The ω-Ti films are grown epitaxially on the epitaxial (111) surface of α-Fe buffer layer on Si substrate at 300 K. Fig.8 shows the XRD patterns of 35 and 50 nm thick Ti films, which are detected to be ω-Ti and α-Ti, respectively. The ω-Ti film is stable until the thickness reaches 40 nm, despite the large lattice mismatch between ω-Ti and α-Fe (about 12%). The authors attributed the formation of ω-Ti film to second-nearest-neighbour atomic interaction at the interface.

Kong et al[36] reported the preparation of nanocrystalline Ti films prepared by DC magnetron sputtering and evaporation on copper foil substrates cooled down to liquid N_2 temperature. The XRD and SAED patterns (Fig.9) show that the crystal structure of sputtered Ti films is β-Ti, while the evaporated film is hcp equilibrium structure. The average grain size of titanium nanocrystalline particles is 6.15±0.18 nm evaluated by XRD patterns. The lattice parameter of the room-temperature β-Ti film is measured to be 0.331 78 nm, which is comparable with the high-temperature β-Ti in Table 2. The authors attributed the formation of β-Ti film to the deposition process, but the nucleation mechanism of β-Ti film is still unclear.

3 Face-Centered Cubic Titanium

3.1 Formation and transformation of fcc-Ti film

The experimental confirmation of the existence of fcc-Ti

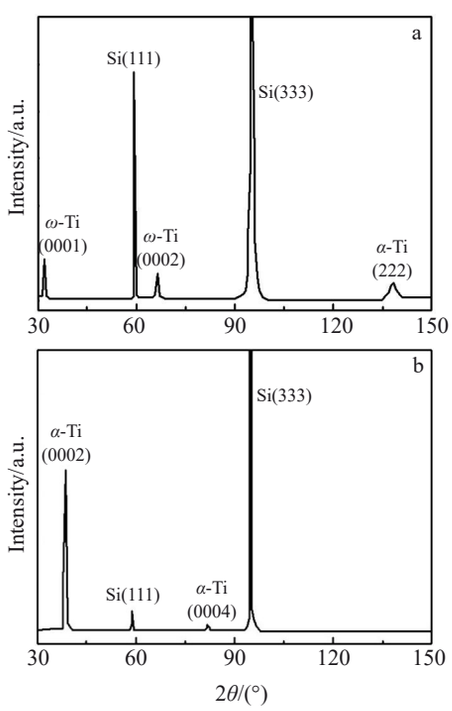

Fig.8 XRD patterns of 35 nm (a) and 50 nm (b) thick Ti thin films deposited on the surface of α-Fe buffer layer on Si substrate[37]

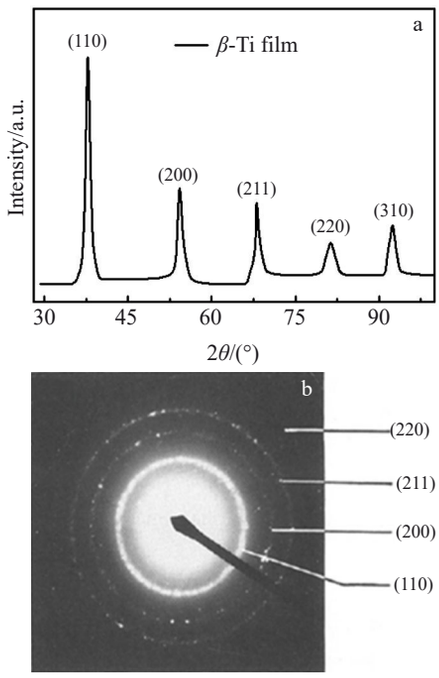

Fig.9 XRD pattern (a) and SAED pattern (b) of sputtered titanium film[36]

was made by Wawner[38] in 1969, who reported the fcc-Ti in a thin film deposited on single crystal NaCl substrate. The fcc structure was thought to arise from pseudomorphic type growth in consistence with proposed misfit theories. At a critical thickness (20~30 nm), there is a transformation from the fcc to the normal hcp structure. This observation opened the gate of investigation of fcc-Ti, and various workers reported similar results for Ti films deposited on various substrates. The stability of fcc epitaxial Ti film depends on the interfacial strain associated with the misfit and the difference in the surface free energy between the film and the substrate materials. Usually, the metastable thin films will transform to the equilibrium structure (α-Ti) when the film thickness reaches a critical value. The experimental data regarding the formation of fcc-Ti obtained by various investigators is summarized in Table 5[56].

In order to find the mechanism of the thickness-dependent fcc→hcp structural transformation, a series of Ti films deposited on SiC(0001) single crystal substrates were prepared using DC magnetron sputtering by Li[56]. Film thickness, sputter power and temperature of deposition were changed to investigate structural transformation. Fig.10 shows the XRD patterns and HRTEM image of the Ti film. The results indicate that the Ti film grows epitaxially with fcc structure, even the thickness is up to about 50 nm. High temperature and low sputter power are propitious to the formation of fcc-Ti. An interesting intermediate state during the fcc→hcp transformation which corresponds to the $(10\bar{1}1)_{\alpha\text{-Ti}}$ X-ray diffraction peak is observed in the HRTEM pattern (area B in Fig. 10b). This intermediate state is also observed in the hcp→fcc transformation of Ti particle by mechanical attrition[79].

Table 5 Experimental data of the fcc-Ti film[56]

Sample	Preparation condition	Critical thickness/nm	Lattice parameter/nm	Ref.
Epitaxial film	NaCl (001) (111)	20~30	0.433	[38]
Epitaxial film	Al (001)	~1.14	0.414 6	[45]
Epitaxial film	Al (110)	0.5~0.6	0.415	[40]
Epitaxial film	SiC (0001)	-	0.438	[50]
Epitaxial film	MgO (001)	4~6	0.425	[49]
Polycrystal	Si (100)	144	0.416 38	[52]
Polycrystal	Si (100)	300	0.420	[55]

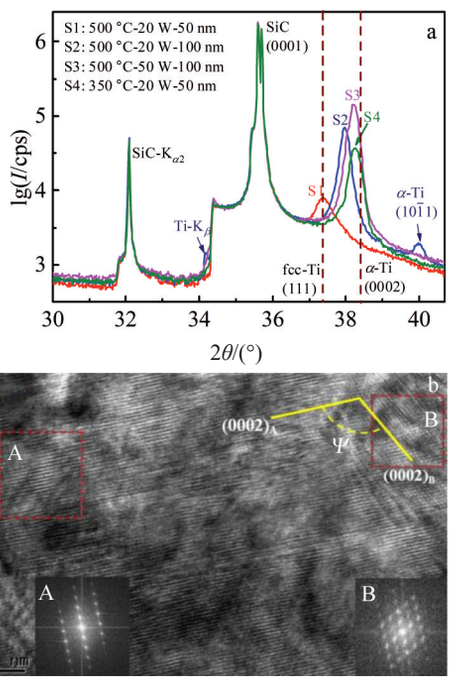

Fig.10 XRD patterns of Ti films deposited under different conditions (a) and HRTEM image of Ti (100 nm)/SiC sample (b)[56]

3.2 Deformation induced hcp-fcc transformation

When titanium underdoes severe plastic deformation, hcp to fcc structural transformation can be activated to accommodate external strain[80]. Recently, many studies reported the observation of deformation induced fcc-Ti by ball mill, compression, tension, cold-rolling and laser shock peening[79-93].

Manna et al[79] reported a metastable hcp→fcc polymorphic structural transformation in titanium powder by mechanical attrition in a planetary ball mill. Fig. 11 shows the XRD patterns of evolution of fcc-Ti produced by mechanical attrition of titanium powder for different time. The continued attrition leads to the decrease in grain size and increase in

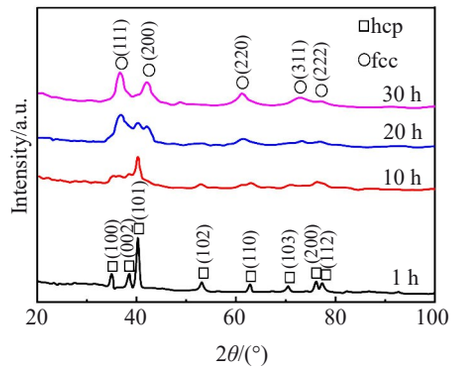

Fig.11 XRD patterns showing evolution structures produced by mechanical attrition of Ti with different accumulation time[79]

lattice parameter, and the appearance of $(111)_{fcc}$ peak after 10 h of attrition. After 30 h of attrition, the whole set of fcc peaks can be observed, which replace the original hcp peaks. Although the authors gave a statement that the $(101)_{hcp}$ peak at 2θ=40.18° disappears completely in the final stage (30 h), we can still see the weak peak at about 2θ=40°. This phenomenon is in accordance with our study on fcc→hcp structural transformation in titanium films. The appearance of 2θ=40° peak indicates an intermediate state of the hcp→fcc structural transformation[56].

The observation of deformation induced hcp→fcc structural transformation in commercial-pure titanium is reported by Hong et al[80] using cryogenic channel-die compression technique. The ultrafine fcc-Ti plate-shaped grains with 70 nm in thickness are found in the intersecting slip bands from the TEM micrograph, as shown in Fig. 12. The HRTEM images and diffract gram based on the fast Fourier transformation (FFT) reveal that the orientation relationship (OR) between the two phases is $<0001>_{hcp}//<001>_{fcc}$, $\{0110\}_{hcp}//\{110\}_{fcc}$ and $\{1120\}_{hcp}//\{110\}_{fcc}$. This OR can be well explained by the proposed hcp→fcc transformation mechanism involving Shockley partial dislocations of $a/6<11\bar{2}0>$ gliding on $\{10\bar{1}0\}$ prism planes.

Wu et al[81] reported the rolling-induced fcc-Ti bands at room temperature in hcp-Ti polycrystalline sample. This hcp→fcc structural transformation offers an additional plastic deformation mode comparable to twinning. The fcc-Ti and hcp-Ti have the OR: $\{10\bar{1}0\}_{hcp}//\{110\}_{fcc}$ and $\langle 0001\rangle_{hcp}//\langle 001\rangle_{fcc}$, which is different from the well-known fcc-hcp orientation relation. The nucleation is via pure-shuffle and the growth is via shear-shuffle mechanisms, different from the established structural transformation path via the collective gliding of Shockley partial dislocations on hexagonal close packed planes.

The hcp→fcc structural transformation is also found in pure titanium samples after thermal deformation or heat treatment. Zhao et al[82] reported structural transformations of commercially pure titanium compressed at 950 °C at different strain rates with thermal simulation. The orthorhombic α'' phase is observed in the intragranular at strain rate of 0.01 s^{-1},

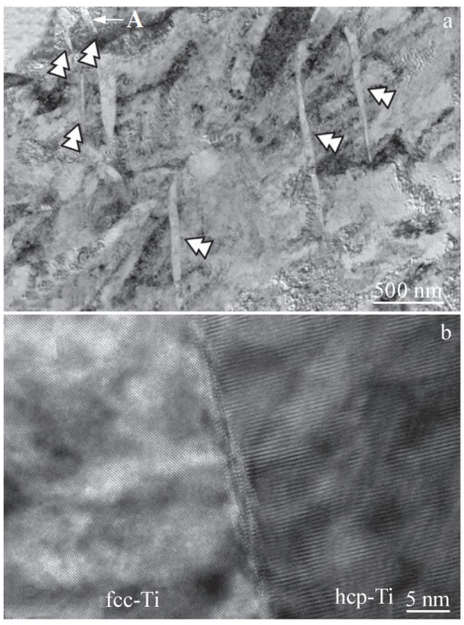

Fig. 12 TEM (a) and HRTEM (b) images of cryogenic channel-die compressed specimen[80]

while the fcc-Ti is produced at strain rate of 10 s^{-1}. The size and amount of both phases increase with the increase in strain rate. Yu et al[83] conducted in-situ TEM study for thin titanium foil at 900 °C. Small precipitates with fcc crystal structure are observed during annealing at approximately 600 °C in the thinner regions of the samples.

Laser shock peening (LSP) is a surface treatment technique by severe plastic deformation with high strain rate of 10^6~10^7 s^{-1}. The pulsed laser can produce a certain shear stress while generating strong dynamic shock pressure, and reduce the phase transformation energy barrier. Recently, we investigated the phase transformations in commercially pure titanium subjected to multiple laser shock peening[84]. As shown in Fig. 13, the LSPed samples undergo $\alpha \rightarrow \omega \rightarrow$fcc$\rightarrow \alpha$ phase transformation as a function of laser shock times. The $\alpha \rightarrow \omega$ phase transformation occurs during the second shock impact. The orientation relationship is $\{0001\}_\omega // \{11\bar{2}0\}_\alpha$, which is consistent with the Silcock pathway. The fcc-Ti appears after the third impact, and the content of fcc-Ti in the samples first increases and then decreases with the impact times. The $\alpha \rightarrow \omega \rightarrow$fcc phase transformations can be attributed to the energy accumulation input by multiple laser shocks, which refines the grains and forms lots of nano mechanical twins. The fcc$\rightarrow \alpha$ reverse transformation may be related to the residual heating which is converted from laser shock energy.

3.3 Deformational behavior of fcc-Ti

The deformational behavior of fcc-Ti was investigated by Yu et al[83]. As shown in Fig. 14, single-phase fcc-Ti, hcp-Ti, and dual-phase hcp/fcc Ti pillars are machined by focused ion beam technology. Nano-compression experiments were carried out at a rate of 2 nm/s. The compressive yield strength of the three pillars is similar, about 1.75 GPa. The maximum compressive stress of two-phase pillar is significantly higher than that of single-phase pillars, which is related to the increase in work hardening rate related to the phase boundary.

Bai et al[85] reported that a large number of fcc-Ti bands with an average width of 0.2 μm and an average length of 6 μm in the high-purity Ti foil are observed after annealing at 500 °C. The annealed foils have excellent capacity of plastic deformation under cold-rolling, which means that the fcc-Ti bands have good plasticity. With the increase of strain, the fcc-Ti undergoes various deformation modes such as shearing, bending, kinking and their combinations, and is transformed to equiaxed grains due to fragmentation and globularization.

3.4 Mechanism of hcp-fcc transformation

The stability of fcc-Ti was calculated by first-principles total-energy, and the results demonstrated that the elastic stability criteria for a cubic crystal are fulfilled by the calculated elastic constants of fcc-Ti[57]. However, the total energy of the fcc-Ti is significantly higher than that of the α-Ti and ω-Ti even with a volume reduction of 15%, as shown in Fig.15.

Ren et al[86] performed molecular dynamics simulations of the hcp-fcc transformation inside the $\{10\bar{1}2\}\langle 10\bar{1}1\rangle$ twinning region in Ti single-crystal nanopillars orientated along [0001] during tension. The hcp-fcc transformation with the orientation relationship of $\langle 0001\rangle_{hcp} \| \langle 001\rangle_{fcc}$ is induced by dislocation glide of multiple Shockley partial dislocations under the condition of size restriction.

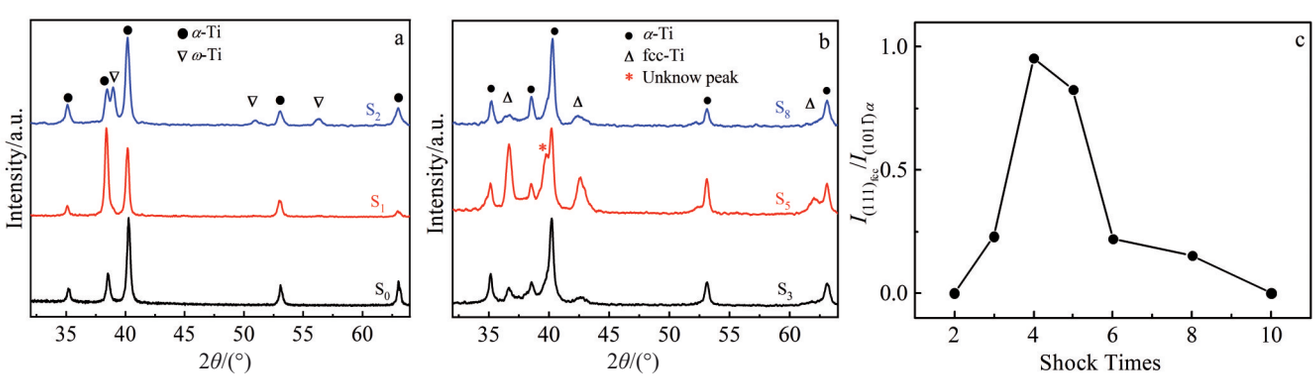

Fig.13 XRD patterns of LSPed samples S_n with different shock times n (a, b) and intensity ratio of $(111)_{fcc}$ and $(10\bar{1}1)_\alpha$ diffraction peaks (c)[84]

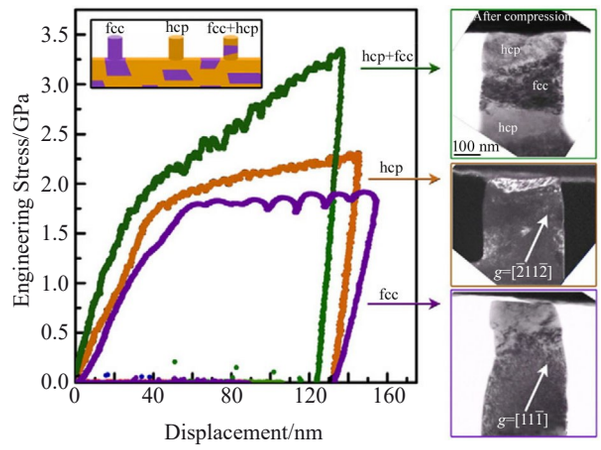

Fig.14 Engineering stress-displacement curves of compression tests on hcp+fcc pillar, hcp pillar and fcc pillar[83]

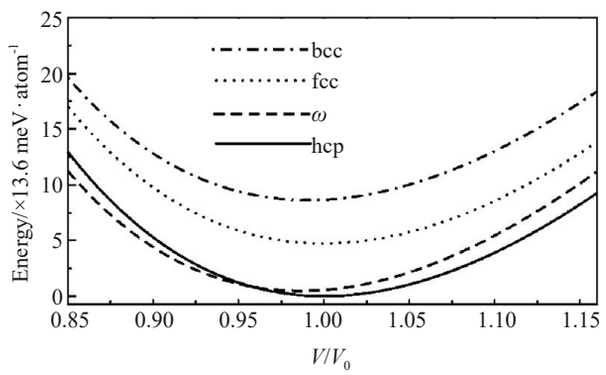

Fig.15 Calculated total energies for the hcp, ω, bcc, and fcc phases of titanium[57]

Zu et al[87] further investigated the phase transformation in Ti nanopillar under [0001] tension using the Zope potential[88]. As shown in Fig. 16, the nucleation and growth of fcc-Ti are accomplished by a glide-shuffle mechanism via glide of atoms every two layers along 1/6<1$\bar{2}$10> plus atomic shuffling.

In order to explain the driving force of hcp-fcc transformation, the total energy difference ΔE between single-phase hcp-Ti and dual-phase hcp/fcc Ti pillars, which is the key criterion of the transformation, can be expressed as:

$$\Delta E=\Delta U_{\text{volume}}+\Delta\gamma_{\text{surface}}+\Delta\gamma_{\text{interface}}+\Delta E_{\text{i}\mu} \quad (1)$$

where ΔU_{volume} is the bulk energy difference between hcp and fcc phases at 0 K, $\Delta\gamma_{\text{surface}}$ is the surface energy difference and $\Delta\gamma_{\text{interface}}$ is the interface energy difference, $\Delta E_{\text{i}\mu}$ is the elastic strain energy difference from the lattice reorientation after phase transformation. Zu et al[87] calculated the bulk potential energy difference ΔU_{volume} as 0.0115 eV/atom, which indicates an increase of bulk energy from the hcp-fcc transformation. Moreover, the interface energy $\gamma_{\text{interface}}$ will increase due to the nucleation and growth of fcc-Ti. Hence, the bulk energy and interface energy cannot be the driving force of the hcp to fcc phase transformation. Therefore, the criterion of hcp-fcc transformation depends on the free surface energy and the lattice strain energy, which is related to the lattice orientation and loading direction.

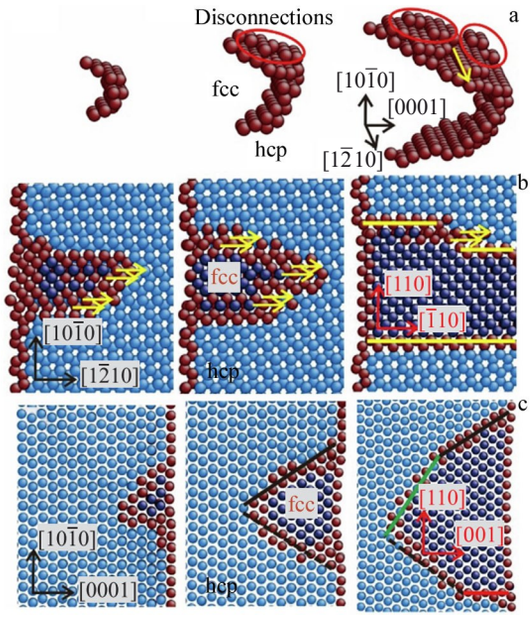

Fig.16 Orientation relationship of $\langle 0001\rangle_{\text{hcp}}//\langle 001\rangle_{\text{fcc}}$ and $\{10\bar{1}0\}_{\text{hcp}}\|\{110\}_{\text{fcc}}$ during the hcp-fcc transformation[87]

4 Conclusions

1) The allotropes of titanium α, β, ω, γ, δ, fcc can be produced by different ways such as high pressure, HPT, laser shock, cold rolling, ultrathin films. We introduced the methods of research and factors of the influence on the structural transformations of titanium, such as temperature, pressure, plastic deformation. Although the calculations predicted the existence of β-Ti under pressure, actually there is no experimental report. The room-temperature β-Ti is only reported in the sputtered Ti films on copper foil substrates cooled down to liquid N_2 temperature.

2) The fcc-Ti can be prepared by film deposition, plastic deformation and heat treatment. However, fcc-Ti bands in bulks are always in nanometer size and dispersed in the titanium matrix, which increase the difficulty of profound research. Researchers investigated the formation process and orientation relationships of fcc-Ti by TEM, HRTEM, XRD, and the phase transformation mechanism by first principles total energy calculation and molecular dynamics simulation. It is confirmed that fcc-Ti can coordinate the plastic deformation and improve the strength.

References

1 Skriver H L. *Physical Review B*[J], 1985, 31(4): 1909
2 Xia H, Parthasarathy G, Luo H *et al*. *Physical Review B*[J], 1990, 42(10): 6736
3 Trinkle D R, Hennig R G, Srinivasan S G *et al*. *Physical Review Letters*[J], 2003, 91: 25 701
4 Jamieson J C. *Science*[J], 1963, 140(3562): 72
5 Ahuja R, Wills J M, Johansson B *et al*. *Physical Review B*[J], 1993, 48(22): 16 269

6 Joshi K D, Jyoti G, Gupta S C *et al*. *Physical Review B*[J], 2002, 65: 52 106

7 Kutepov A L, Kutepova S G. *Physical Review B*[J], 2003, 67: 132 102

8 Ahuja R, Dubrovinsky L, Dubrovinskaia N *et al*. *Physical Review B*[J], 2004, 69: 184 102

9 Hu Q M, Lu S, Yang R. *Physical Review B*[J], 2008, 78: 52 102

10 Mukherjee D, Joshi K D, Gupta S C. *Transactions of the Indian Institute of Metal*[J], 2011, 64: 245

11 Salati A, Mokhtari E, Panjepour M *et al*. *Journal of Physics and Chemistry of Solids*[J], 2013, 74: 584

12 Baruffi C, Finel A, Bouar Y L *et al*. *Computational Materials Science*[J], 2022, 203: 111 057

13 Lin C, Liu Z L, Yin G L. *Rare Metal Materials and Engineering*[J], 2008, 37(4): 571

14 Jayaraman A, Klement W, Kennedy G C. *Physical Review*[J], 1963, 131(2): 644

15 Sargent G A, Conrad H. *Materials Science & Engineering*[J], 1971, 7(4): 220

16 Akahama Y, Kobayashi M, Kawamura H. *Journal of the Physical Society of Japan*[J], 1990, 59(11): 3843

17 Xia H, Duclos S J, Ruoff A L *et al*. *Physical Review Letters*[J], 1990, 64: 204

18 Xia H, Ruoff A L, Vohra Y K. *Physical Review B*[J], 1991, 44 (18): 10 374

19 Vohra Y K, Spencer P T. *Physical Review Letters*[J], 2001, 86: 3068

20 Akahama Y, Kawamura H, Bihan T L. *Physical Review Letters*[J], 2001, 87: 275 503

21 Joshi K D, Jyoti G, Gupta S C *et al*. *Journal of Physics Condensed Matter*[J], 2002, 141(44): 10921

22 Errandonea D, Meng Y, Somayazulu M *et al*. *Physica B: Condensed Matter*[J], 2005, 355: 116

23 Velisavljevic N, Jacobsen M, Vohra Y. *Materials Research Express*[J], 2014, 1: 35 044

24 Li S, Yuan Q, Zhang J *et al*. *Journal of Alloys and Compounds*[J], 2022, 906: 164 312

25 Perez-Prado M T, Zhilyaev A P. *Physical Review Letters*[J], 2009, 102: 175 504

26 Srinivasarao B, Zhilyaev A P, Perez-Prado M T. *Scripta Materialia*[J], 2011, 65: 241

27 Kilmametov A R, Khristoforov A V, Wilde G *et al*. *Tenth European Powder Diffraction Conference*[J], 2007, 26: 339

28 Todaka Y, Sasaki J, Moto T *et al*. *Scripta Materialia*[J], 2008, 59: 615

29 Edalati K, Matsubara E, Horita Z. *Metallurgical and Materials Transactions A*[J], 2009, 40: 2079

30 Wang C T, Fox A G, Langdon T G. *Journal of Materails Science*[J], 2014, 49: 6558

31 Edalati K, Daio T, Arita M *et al*. *Acta Materialia*[J], 2014, 68: 207

32 Edalati K, Horita Z. *IOP Conference Series: Materials Science and Engineering*[J], 2014, 63: 12 099

33 Sinha S, Sahu V K, Beura V *et al*. *Materials Science & Engineering A*[J], 2021, 802: 140 687

34 Feibelman P J, Appelbaum J A, Hamann D R. *Physical Review B*[J], 1979, 20: 1433

35 Huang J C A, Du R R, Flynn C P. *Physical Review Letters*[J], 1991, 66: 341

36 Kong J, Shen H, Chen B *et al*. *Thin Solid Films*[J], 1992, 207: 51

37 Cheng Y T, Meng W J. *Physical Review Letters*[J], 1996, 76: 3999

38 Wawner F E, Lawless K R. *Journal of Vacuum Science & Technology*[J], 1969, 6: 588

39 Saleh A A, Shutthanandan V, Smith R J. *Journal of Vacuum Science & Technology A*[J], 1992, 11: 1982

40 Saleh A A, Shutthanandan V, Smith R J. *Physical Review B*[J], 1994, 49: 4908

41 Kim S K, Jona F, Marcus P M. *Journal of Physics: Condensed Matter*[J], 1996, 8: 25

42 Tepper T, Shechtman D, Heerden D V *et al. Materials Letters*[J], 1997, 33: 181

43 Harada T, Ohkoshi H. *Journal of Crystal Growth*[J], 1997, 171: 433

44 Marcus P M, Jona F. *Journal of Physics: Condensed Matter*[J], 1997, 9: 6241

45 Saleh A A, Shutthanandan V, Shivaparan N R *et al*. *Physical Review B*[J], 1997, 56: 9841

46 Smith R J, Kim Y W, Shivaparan N R *et al*. *Surface and Interface Analysis*[J], 1999, 27: 185

47 Lai J B, Chen L J, Liu C S. *Micron*[J], 1999, 30(3): 205

48 Hara S. *Applied Surface Science*[J], 2000, 162: 19

49 Kado T. *Surface Science*[J], 2000, 454-456: 783

50 Sugawara Y, Shibata N, Hara S *et al*. *Journal of Materials Research*[J], 2000, 15: 2121

51 Teraji T, Hara S. *Physical Review B*[J], 2004, 70: 35 312

52 Chakraborty J, Kumar K, Ranjan R *et al*. *Acta Materialia*[J], 2011, 59: 2615

53 Chen Y, Feng X, Kasukabe Y *et al*. *Journal of Alloys and Compounds*[J], 2013, 577: 18

54 Arshi N, Lu J, Lee C G *et al*. *Bulletin of Materials Science*[J], 2013, 36: 807

55 Fazio M, Vega D, Kleiman A *et al*. *Thin Solid Films*[J], 2015, 593: 110

56 Li L, Liu Y, Mao X *et al*. *Materials Characterization*[J], 2017, 134: 64

57 Aguayo A, Murrieta G, Coss R D. *Physical Review B*[J], 2002, 65: 92 106

58 Ikehata H, Nagasako N, Furuta T *et al. Physical Review B*[J], 2004, 70: 174 113

59 Akahama Y, Kobayashi M, Kawamura H. *Journal of the Physical Society of Japan*[J], 1990, 59: 3843

60 Matthias B T. *Physical Review*[J], 1955, 97: 74
61 Silcock J M, Davies M H, Hardy H K. *Nature*[J], 1955, 175: 731
62 Chang H, Zhou L, Zhang T J. *Rare Metal Materials and Engineering*[J], 2007, 36(9): 1505 (in Chinese)
63 Zhang Z X, Lei M, Wan M P *et al. Rare Metal Materials and Engineering*[J], 2017, 46(11): 3277
64 Wang C L, Li F, Chen F W *et al*. *Rare Metal Materials and Engineering*[J], 2019, 48(12): 3917 (in Chinese)
65 Bagaryatskiy Y A, Nosova G I, Tagunova T V. *Doklady Akad Nauk SSSR*[J], 1958, 122: 593
66 Hu C E, Zeng Z Y, Zhang L *et al*. *Journal of Applied Physics*[J], 2010, 107: 93 509
67 Bychkov Y F, Likhanin Y N, Maltsev V A. *Fiz Metal Metalloved*[J], 1974, 38: 1294
68 Vohra Y K, Sikka S K, Vaidya S N *et al*. *Journal of Physics and Chemistry of Solids*[J], 1977, 38: 1293
69 Hennig R G, Trinkle D R, Bouchet J *et al*. *Nature Materials*[J], 2005, 4: 129
70 Cerreta E, Gray G T, Lawson A C *et al*. *Journal of Applied Physics*[J], 2006, 100: 13 530
71 Silcock J M. *Acta Metallurgica*[J], 1958, 6(7): 481
72 Vohra Y K, Menon E S, Sikka S K *et al*. *Acta Metallurgica*[J], 1981, 29(2): 457
73 Sikka S K, Vohra Y K, Chidambaram R. *Progress in Materials Science*[J], 1982, 27(3-4): 245
74 Saxena A K, Kaushik T C, Gupta S C. *Journal of Applied Physics*[J], 2015, 118: 1
75 Razorenov S V, Utkin A V, Kanel G I. *High Pressure Research*[J], 1995, 13: 367
76 Borisenok V A, Zhernokletov M V, Kovalev A E. *Combustion, Explosion, and Shock Waves*[J], 2014, 50: 346
77 Zong H, Ding X, Lookman T *et al*. *Acta Materialia*[J], 2016, 115: 1
78 Li L, Jia W, Ji V. *Vacuum*[J], 2022, 206: 111 510
79 Manna I, Chattopadhyay P P, Nandi P *et al*. *Journal of Applied Physics*[J], 2003, 93(3): 1520
80 Hong D H, Lee T W, Lim S H *et al*. *Scripta Materialia*[J], 2013, 69: 405
81 Wu H C, Kumar A, Wang J *et al*. *Scientific Reports*[J], 2016, 6: 24 370
82 Zhao H L, Hu X Y, Song M *et al*. *Scripta Materialia*[J], 2017, 132: 63
83 Yu Q, Kacher J, Gammer C *et al*. *Scripta Materialia*[J], 2017, 140: 9
84 Li L, Jia W, Ji V. *Surface and Coatings Technology*[J], 2022, 450: 129 010
85 Bai F, Yin L, Zhao W *et al*. *Materials Science & Engineering A*[J], 2021, 800: 140 287
86 Ren J, Sun Q, Xiao L *et al*. *Computational Materials Science*[J], 2014, 92: 8
87 Zu Q, Guo Y F, Yao X. *Applied Surface Science*[J], 2020, 509: 145 234
88 Zope R R, Mishin Y. *Physical Review B*[J], 2003, 68: 24 102
89 Chen C, Qian S F, Wang S *et al. Materials Characterization*[J], 2018, 136: 257
90 Zheng X D, Gong M Y, Xiong T *et al*. *Scripta Materialia*[J], 2019, 162: 326
91 Li F X, Chen P, Chen Z *et al*. *Journal of Alloys and Compounds*[J], 2019, 806: 939
92 Hao P D, Chen P, Deng L *et al*. *Journal of Materials Research and Technology*[J], 2020, 9(3): 3488
93 Zhao Z P, Zhu G M, Kang Y L *et al. Journal of Alloys and Compounds*[J], 2020, 815: 152 298

钛的晶体结构和结构转变研究进展

李 磊[1]，郭荻子[1]，应 扬[1]，洪 权[1]，Vincent JI[2]
(1. 西北有色金属研究院，陕西 西安 710016)
(2. 巴黎萨克雷大学，法国 奥赛 91405)

摘 要：钛具有高强度，低密度，耐腐蚀等特性，并在多个领域得到应用。多年来，钛的同素异构体的晶体结构和结构转变受到了学者的广泛关注。除了密排六方结构的平衡相（α-Ti），面心立方结构的高温相（β-Ti）和六方结构的高压相（ω-Ti）外，学者通过各种方法尝试在极端条件下制备钛的其他亚稳相结构。在过去的几十年中，人们在超高压条件下发现了γ-Ti和δ-Ti，并通过高压扭转实验、激光冲击实验和超薄薄膜实验等方法制备了在室温条件下可以稳定存在的ω-Ti和fcc-Ti。综述了钛的同素异构体（不包括合金）的晶体结构和结构转变类型，并介绍了不同结构钛的稳定性以及结构转变机理。

关键词：晶体结构；结构转变；高压；面心立方钛

作者简介：李 磊，男，1983年生，博士，研究员，西北有色金属研究院，陕西 西安 710016，电话：029-86250729，E-mail：lilei@c-nin.com